The AO in AOF

Sylvain Oberti[a], Johann Kolb[a], Pierre-Yves Madec[a], Pierre Haguenauer[a], Miska Le Louarn[a], Lorenzo Pettazzi[a], Andres Guesalaga[b], Robert Donaldson[a], Christian Soenke[a], Bogdan Jeram[a], Marcos Suárez Valles[a], Mario Kiekebusch[a], Javier Argomedo[a], Paolo La Penna[a], Jerome Paufique[a], Robin Arsenault[a], Norbert Hubin[a], Joel Vernet[a]

[a]European Southern Observatory, Karl-Schwarzschild-Strasse, 2, 85748 Garching-bei-München

[b]Pontificia Universidad Católica de Chile, Av Libertador Bernardo O'Higgins 340, Santiago, Chile

ABSTRACT

The long commissioning of the Adaptive Optics Facility (AOF) project has been completed shortly after this conference, providing AO correction to two Very Large Telescope (VLT) foci supported by an adaptive secondary mirror and four laser guide stars. Four AO modes are delivered: a Single Conjugate AO (SCAO) system for commissioning purpose, wide field and medium field Ground Layer AO (GLAO) for seeing improvement and narrow field Laser Tomography AO (LTAO) for ultimate performance. This paper intends to describe the implemented AO baseline and to highlight the most relevant results and lessons learned. In particular, it will address the control and reconstruction strategy, the wavefront sensing baseline and the online telemetry used to optimize the system online, estimate the turbulence profile and calibrate the misregistrations. Focusing on the LTAO mode, we will describe the tomography optimization, by exploring the reconstruction parameter space. Finally, on sky performance results will be presented both in terms of strehl ratio and limiting magnitude

Keywords: Adaptive Optics Facility, Ground Layer Adaptive Optics, Laser Tomography Adaptive Optics, Tomography, Reconstruction, Regularization, Online telemetry, Pseudo-synthetic Interaction Matrix, Misregistration, Adaptive vibration tracking and cancellation, GRAAL, GALACSI, MUSE, DSM, 4LGSF, SPARTA, ASSIST

1. INTRODUCTION

The AOF [1] is a project that was initiated in 2006. Twelve years later, the full suite of AO and associated instrumental modes has been commissioned, transforming VLT's Unitary Telescope number 4 (UT4) into an adaptive telescope [2][3][4]. Meanwhile, the following subsystems have been designed, built, tuned, verified and delivered:

- The 4 Laser Guide Star Facility (4LGSF) [5] consisting of four lasers of 20W coupled to four individual launch telescope mounted around M1 centerpiece.
- The Deformable Secondary Mirror (DSM) [6] replacing the formerly monolithic M2 and providing adaptive correction within the telescope at 1kHz over 1156 degrees of freedom in the pupil plane.
- At Nasmyth A: the GRAAL AO module [7] incorporating a 40x40 NGS SCAO mode used for commissioning purpose (not described here) and a large field GLAO module (7' LGS diameter) providing a uniform ensquared energy improvement over the field of view to the K band imager HAWK-I [8].
- At Nasmyth B: the GALACSI AO module serving the integral field spectrograph MUSE [10] [11] delivering data cubes in the optical wavelength domain. GALACSI offers a medium FoV (2' LGS diameter) GLAO mode providing seeing improvement to MUSE for its Wide Field Mode (WFM: 1' square), typically reducing the PSF full width at half maximum (fwhm) by a factor of two. In addition, GALACSI offers an LTAO mode providing the ultimate performance at the center of the MUSE field in Narrow Field Mode (NFM : 7.5" square), that is to say a close to diffraction limit PSF in the visible, with a Strehl ratio of more than 5% at 650 nm.

This paper will not describe the AOF control strategy nor its complex and very efficient acquisition sequence as it was already presented in the past [12]. Instead, we would like to focus here on some AO aspects which may be relevant to the community, because they are novel and/or directly applicable to the ELT AO systems. The LTAO mode will be particularly highlighted here because it is the most challenging and sensitive AO system delivered by the AOF project.

2. WAVEFRONT SENSING

The wavefront sensors are providing the fundamental wavefront measurements used to perform the tomographic reconstruction, to compute the diagnostics based on telemetry data such as C_n^2 profiling and to characterize and cancel vibrations. The high order loop is managed by four laser guide star wave front sensor composed of 40x40 subaperture, taking care of the control of all modes but Tip/Tilt. The natural guide star wavefront sensing is dedicated to the compensation of fast Tip/Tilt but also used for truth sensing of the low order modes (defocus and astigmatisms).

2.1 Laser Guide Star wavefront sensors (LGS WFS)

The design of the LGS WFS is a key element of success of the AOF. Indeed, the technologies (CCD220, 4LGSF) developed in the frame work of the AOF project have allowed to reach a situation where the LGS WFS is linear, unbiased and operated in a good Signal to Noise Ratio (SNR) regime. The reasons for this are the following:

- The LGS spots are well sampled, without truncation because:
    - There are 6x6 pixels per subaperture with a pixel scale of 0.83".
    - The LGS spot size (small axis) typically exhibits a fwhm of 1.5", hence it is well sampled with almost 2 pixels per fwhm. Let us remind that undersampling is not significantly penalizing the non-linearity of the WFS response up to 1 pixel per fwhm [13].
    - The spot elongation on an 8 m telescope with a side launch is not a big issue. Indeed, we typically observe an elongation of 2.5" fwhm in the subaperture located at the furthest distance from the launch telescope. Moreover, in the theoretical worst case of a very wide sodium layer (22 km) observed at zenith, the spot elongation remains smaller than 6 pixels, which is the field of view of our LGS WFS.
    - The good optical quality of the LGS optical path allows working with small slopes offsets. The slopes offsets are calibrated with an artificial source located at the input focal plane of the LGS WFSs. This calibration accounts only for the non-common path aberrations from the WFS path. The LGS WFS slopes offset are significantly smaller than 0.3 pixels, which is the maximum value measured for subapertures located at the edge of the pupil, whose illumination is so truncated that these subapertures are discarded. The standard deviation over the full vector of 2480 slopes per WFS is around 0.04 pixels, so very small.
    - A small residual jitter is achieved by means of a uplink jitter control, with a jitter actuator located either in the laser launch telescope (GRAAL case) or in a pupil plane within the LGS WFS optical path (GALACSI case), proving residuals of respectively less than 150 mas and 60 mas by design.
    - For the 3 reasons listed above, LGS spot truncation virtually never occurs in closed loop operation
- The measurement SNR is good because:
    - The LGS return flux is high, with 2 to 4 times more photons than expected at the time of design, with 6 to 30 million photons/m2/s depending on the zenith distance and the azimuthal angle. In practice, we get between 100 and 400 photons per subaperture per ms while the system was designed to work with 88 photons per subaperture per ms and capable of dealing with 4 times less photons. This flux level can be attained in case of strong cloud overcast, which generally leads to telescope closure due to a too high humidity rate. In other words, the High Order (HO) loop can be closed with lasers almost all the time. Only very low elevation angles, below 30° are not accessible.
    - The CCD220 provides sub-electron Read-Out Noise (RON).
    - In these good SNR conditions, there is no interest in using advanced centroiding algorithm. Even though the design baseline was to work with a weighted center of gravity, the AO modules have been commissioned and delivered with a classical center of gravity, thresholded at 3 sigmas of RON. The advantages of this solution are that the slope response is linear over a wide dynamic range and that the

design plate scale is preserved when converting the slopes to wavefront. Furthermore, the classical center of gravity does not need to be updated online according to seeing or spot size in general.

Overall, the AOF has been blessed with high order WFSs which are unbiased, linear, robust and performing in good SNR regime. As a consequence, simulating the WFSs in a synthetic model is straight-forward.

2.2 Natural guide star wavefront sensors (NGS WFS)

The fast Tip/Tilt is measured by an NGS WFS, an off axis full pupil visible imager in the case of the two GLAO modes and an on axis (within 3.5") 2x2 J-H band Shack-Hartmann for the LTAO mode. In all modes, a truth sensor is used in a cascade control scheme to track the slow varying defocus, including a contribution from the sodium layer altitude variation. For the LTAO mode, the on axis 2x2 WFS is used as a truth sensor for defocus and astigmatisms while the active optics Shack-Hartmann plays this role for the two GLAO modes.

In order to maximize the sky coverage, the Tip/Tilt measurement is performed via an optimized weighted center of gravity. The weighting function is an elliptical gaussian of twice the fwhm of the spot. To generate and then update the weighting function according to spot size in order to account for seeing variation, HO loop performance variation and object shape, the NGS spot is fitted by an RTC object called spot monitor. The spot monitor periodically performs an elliptical gaussian fit on the average image and generates the weighting map. The spot size is stored for future trending. The automatic generation of weighting maps is an essential tool when guiding on extended targets for the LTAO mode. Indeed, it is not always possible to anticipate the shape of the target object and to pre-generate the weighting maps.

Furthermore, to perform best in low flux condition (limiting magnitude), it is essential to subtract the dark and background map from the pixel intensity vector, otherwise the centroid will be strongly biased. The evolution of the sum of the dark and background is tracked by a background follower algorithm that estimates the offset to be applied in each detector read-out channel by tracking the intensity of well chosen "dark" pixels.

2.3 LGS spot monitor

A similar spot monitor object was implemented for the LGS WFS. Initially, the objective was also to be able to update the weighting maps online in order to optimize the system performance in low flux conditions. Finally, the weighted center of gravity has been discarded as explained above. However, the spot monitor functionality remains and allows fitting the LGS spots in each subaperture. A 2D moffat fit is performed on the LGS spots short exposure. Assuming laser launch telescope coordinates with respect to the pupil plane, the fit can be performed on a full individual frame. The LGS spot monitor generates weighting maps (see Figure 1). The LGS size (small axis) and Sodium layer thickness are extracted, logged and trended during every observation.

An LGS dark follower algorithm is tracking the bias evolution in each of the 8 read-out channels of the CCD220. The temporal average of the spatial median intensity is computed in pixel areas that appear in the left image of Figure 1.

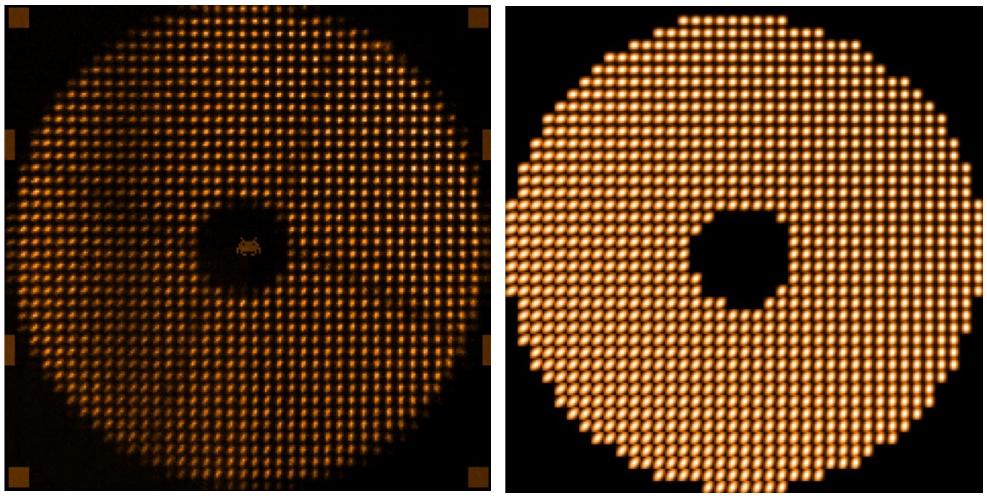

Figure 1: LGS spot monitor [Left] 1 s averaged pixel frame where the dark follower sensing areas appear in the corners and in the center of the frame [Right] Result of the 2D Moffat fit of the LGS spot in all subapertures

Finally, it is interesting to note its is possible to perform some relevant flux statistics with a single frame of LGS WFS. With 1240 subapertures in each WFS, it is possible to evaluate in each frame if the LGS flux is higher than a predefined threshold in a significant number of subapertures. Otherwise, the HO loop is frozen, which is equivalent to setting the integral gain to 0, until the flux exceeds again the threshold. This way, the HO loop is extremely robust to any flux drop (aircraft avoidance, thick cloud, vignetting).

3. TELEMETRY AND VIBRATION MANAGEMENT

Telemetry data is used to estimate a large number of parameters [14] which are logged and can be used for future trending or attached to the scientific data for further analysis (PSF reconstruction for example).

3.1 Atmospheric parameters estimation

The real time data (closed loop DM commands and WFS slopes) is used to compute the wavefront variance corrected by the deformable mirror and the uncorrected variance seen in the WFS residual slopes. The pseudo-open loop slopes are calculated in order to estimate the seeing, the outer scale, but also the fraction of turbulence in the ground layer (only for the GLAO modes) and the gain in wavefront error reduction. The seeing estimation has proven to be consistent with the seeing estimates provided by the DIMM (see **Figure 2**)

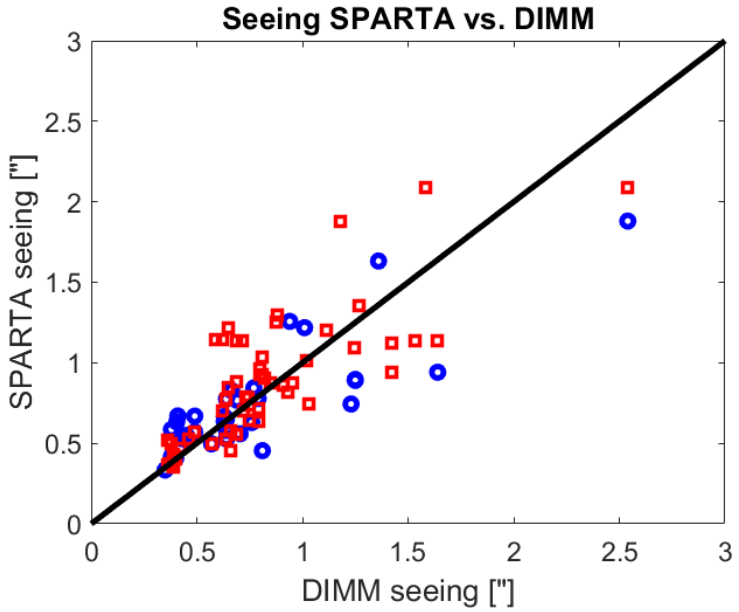

Figure 2: Seeing estimated by AOF SPARTA vs. DIMM seeing along the line of sight at 500nm in mode LTAO [Red] and GLAO[Blue]

Thanks to two of the four LGS WFSs, a slodar approach ([15],[16]) can be applied in order to estimate the C_n^2 profiles. This algorithm is deployed in each LGS AO mode with a different field depth and z resolution, sensing up to 2 km for GRAAL (7' dimeter) and 20 km for GALACSI NFM (20" diameter). This information is crucial to analyze the performance achieved during commissioning. The C_n^2 profile is attached to the scientific data. In particular, it can be used for PSF reconstruction. Ultimately, the C_n^2 profile can be used to judge the pertinence of an OB and reschedule in real time. For example, if during a MUSE WFM OB the ground layer is identified as weak and the seeing good enough, the instrument responsible may decide to switch to NFM (LTAO mode) to perform the next OB.

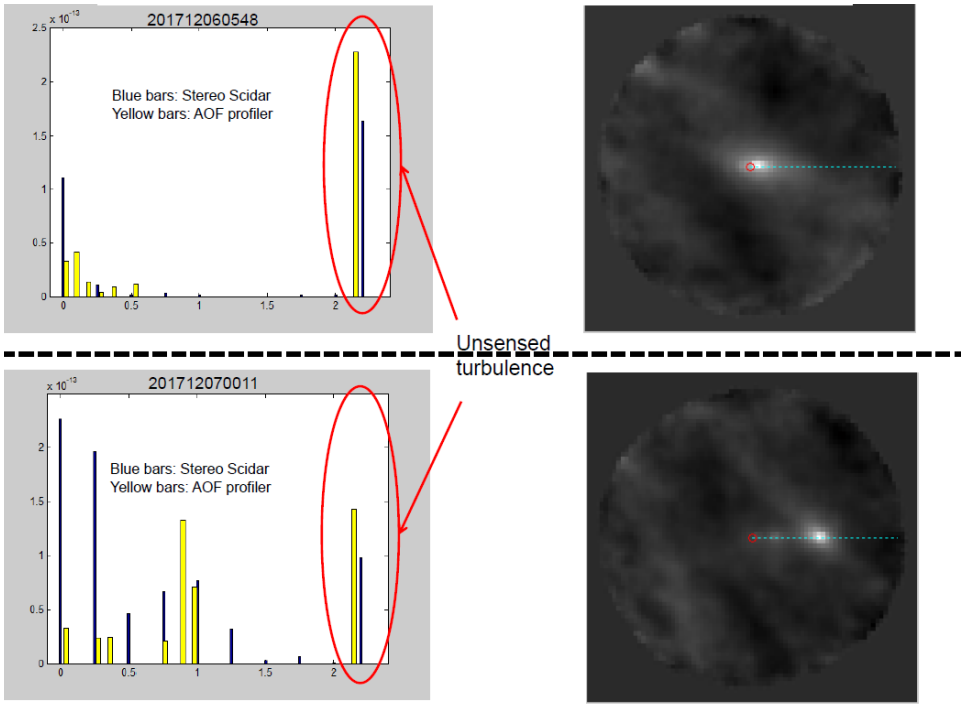

Figure 3: Example of Cn2 profile provided by GRAAL, closely simultaneous with stereo scidar. In this wide field mode, only the first 2 kms of turbulence are sensed with a good resolution. A first validation has been performed by comparing with the stereo-scidar measurements. [Top] Case where most of the energy within the first 2 kms is located at the ground [Bottom] Case where a significant layer is located around 1km, which appears clearly in the slopes covariance map [Right]

3.2 Vibration management

For GALACSI NFM, the Adaptive Vibration Cancellation algorithm (AVC [17]) allows tracking the amplitude, phase and frequency of vibration peaks that can be seen by the NGS WFS (Tip, Tilt and Defocus). The algorithm was implemented, tested and successfully validated in the laboratory on the ASSIST ([18][19][20]) bench where the environment was not quiet. For example, a strong vibration peak along the tip mode could be cancelled, reducing the cumulative power by a factor larger than 3 as one can see on the left plot of Figure 4. The performance of the AVC was confirmed by witnessing strehl ratio improvement on the corrected PSFs. Finally, it was proven that the algorithm can deal with vibrations that are rotating with respect to the pupil plane. At the VLT, the vibrational environment is more friendly than on ASSIST. On the right plot of Figure 4, one can see that he tip vibration is weaker and that AVC correction only brings a moderate improvement. The situation is similar for Tilt and Defocus. Actually, the dominating vibration occurs along the 2 trefoils at a frequency of about 45 Hz. Furthermore, the trefoil vibrations are aliased on the measurements of defocus and astigmatisms provided by the 2x2 Shack-Hartmann, hence we cannot really trust these measurements to track vibrations. The aliasing was verified by applying a trefoil vibration disturbance to the DSM. Finally, it is hard to manage vibrations efficiently when the NGS WFS is operated around its faint limit. So, it was decided to kill the trefoil vibration by applying a specifically designed temporal filter to the high order loop temporal controller, so to introduce a notch at 45 Hz in the rejection transfer function. Figure 5 shows that the 40 nm rms of vibration along each trefoil mode is reduced to less than 10 nm with the notch of 20 dB damping. The trefoil vibration correction also yields an improvement of the cumulative PSD of the defocus and astigmatisms where the residual trefoil is aliased.

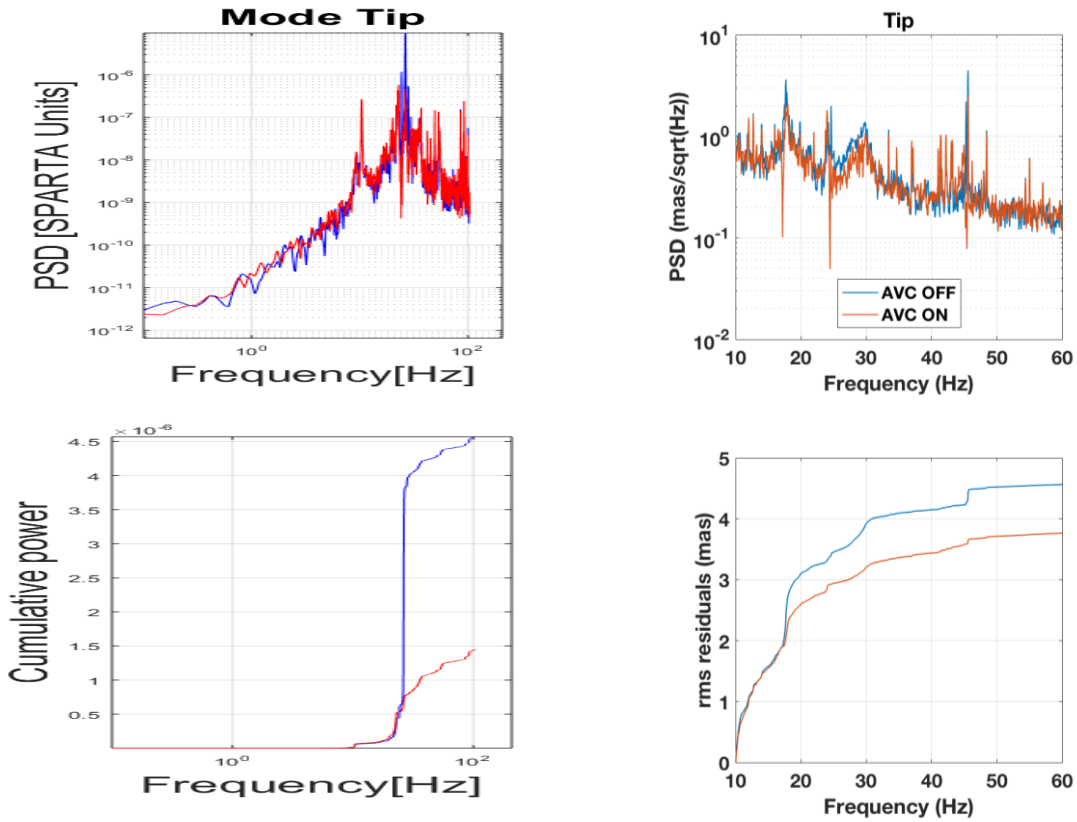

Figure 4:[Left] Laboratory results obtained on ASSIST with a strong vibration peak [Right] Results on sky at the VLT [Top] Power Spectrum Densities along mode Tip with AVC OFF (blue) and ON (red) [Bottom] cumulative PSDs in variance (left) and rms (right)

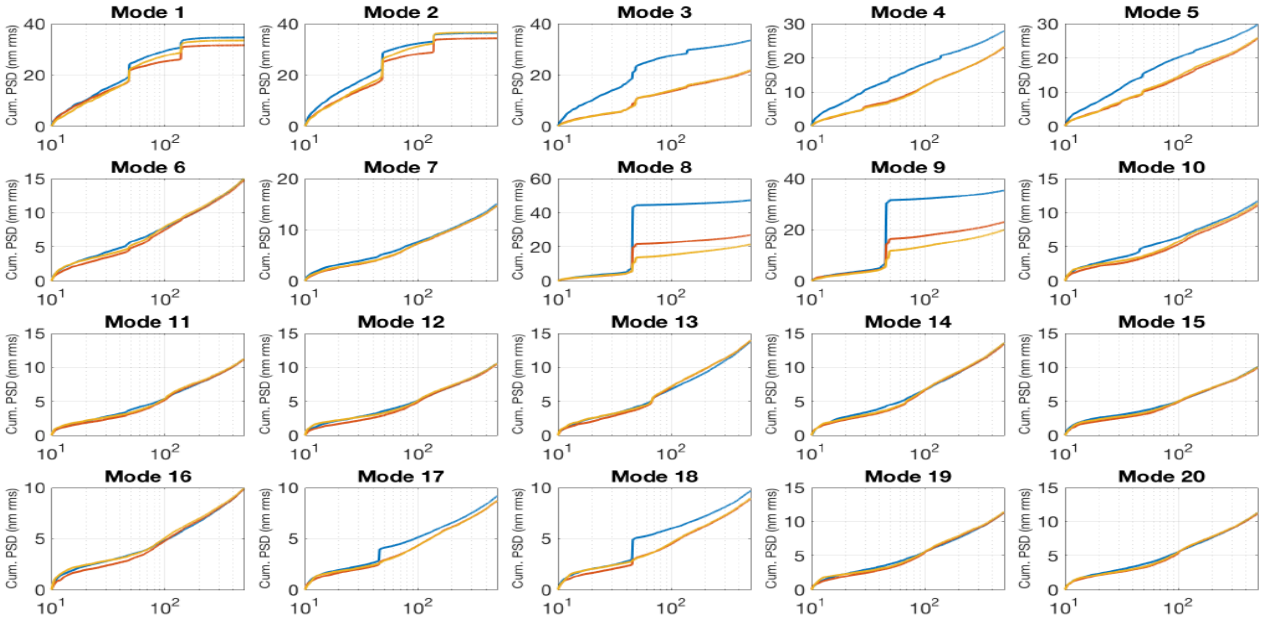

Figure 5: Vibration rejection by applying a 45 Hz notch filter in the HO loop controller - Cumulative PSD for the 20 first Zernike modes - mode 1 and 2 are Tip and Tilt - mode 3 is Defocus - mode 4 and 5 are the 3rd order astigmatisms – mode 8 and 9 are the trefoils – [Blue] No correction [Red] 12 dB damping [Yellow] 20 dB damping

4. WAVEFRONT RECONSTRUCTION

In this section, we will describe the approach chosen to build the LGS tomographic reconstructor, based on a Pseudo Synthetic Interaction Matrix model (PSIM [21]). In particular, the focus will be set on the tuning of the LTAO reconstructor model.

4.1 Pseudo-synthetic interaction matrix

The DM being the secondary mirror of the telescope, there is no artificial calibration source allowing to measure an interaction matrix as done classically for AO systems. Two options remain to estimate the interaction between the DM actuators and the WFS measurements as described in [24]:

- A synthetic model of the system: this is the AOF baseline for the HO loop. It has been validated in the lab and on sky.
- A measurement on sky: this is the baseline for the LO loop. The interaction matrix is measured on sky by fast modal push and pulls. HO interaction matrix are also measured on sky during commissioning to tune the synthetic models. It can be done by fast push-pull [23] or synchronous detection of a modal harmonic modulation [25]

The high order interaction matrix is built with a PSIM based on the two elements listed above. Some measurements performed in the lab and on sky allow tuning the synthetic model by incorporating the following ingredients:

- The DM model: For AOF, the DM model is reliable as the voice-coil technology ensures an accurate knowledge of the mirror shape thanks to a fast local control loop. As a matter of fact, the commissioned model is based on influence functions estimated by Finite Element Analysis. In the laboratory, the influence functions were measured and the quality of the Finite Element Model was validated. The influence function shape depends only on the mechanical properties of the glass shell and can therefore be considered constant in time. Nevertheless, a gain per actuator may appear as the capacitive sensors used to control each actuator position may age. So far, such behavior has not been witnessed on AOF and the gains are all equal to 1. With an up to date list of valid actuators, the influence functions are used to calculate the Karhunen-Loewe modal basis used to invert the interaction matrix.
- The LGS WFSs model: This model is fairly straight forward as our LGS WFSs are linear and unbiased (see section 2.1). Our model is based on a geometrical model of the Shack-Hartmann WFS. For each LGS WFS, a mask of useful subapertures is defined based on photometric and noise measurements. Provisions have been considered to introduce an optical gain per subaperture depending on the spot size and the centroiding algorithm. It is finally not used as our slope response remains stable with a classical center of gravity.
- The misregistrations, in other words the effect of optical propagation when imaging the DM actuator pattern (pupil plane) onto each of the four lenslet arrays. No analog device has been planned to control the shifts. Thus, our strategy is to include them in our pseudo-synthetic model. The advantage of this numerical approach is that we can go beyond the pupil shifts and also manage the clocking angle and the pupil magnification including anamorphose. In principle, a calibrated pupil distortion can also be included into the numerical model even if it is not done for AOF yet.

Once tuned in commissioning, the pseudo-synthetic model does not require any additional daytime or night time calibration. Since it is noise free, it is easy to invert and allows controlling high order spatial frequencies, essentially almost all the degrees of freedom of the DSM Finally, as it can be computed on demand in the RTC cluster, the reconstructor can be adapted to varying misregistrations. The DM and WFS models being straight forward, we will now focus on the way to estimate and manage the misregistration term. The baseline strategy to measure the misregistrations in AOF is to project the interaction matrix onto sensitivity matrices representative of the effect of pupil shifts, rotation and stretch [22]. In closed loop operation, a noisy version of the interaction matrix can be retrieved by cross-correlating the delta slopes and delta commands [26]. We do not need to reach a high SNR in order to estimate the 5 misregistration parameters accurately.

4.2 Misregistration management

The AOF is an interesting case because at each of the two Nasmyth foci populated with an LGS AO module, the behavior in terms of misregistration is significantly different. As a result, two different strategies have been applied.

We will start by describing the GRAAL case. GRAAL is attached to the Nasmyth adaptor rotator and HAWK-I is attached to GRAAL. Both modules rotate together with the adaptor rotator in field tracking mode. In order to keep the GRAAL LGS WFSs coaligned with the LGSs and with the DSM, a corotator is hosting the 4 LGS WFSs and rotates in pupil minus field tracking mode. In addition to the DSM flexure depending on its orientation w.r.t gravity, hence telescope elevation angle, 3 axes are involved in the generation of dynamic misregistrations in GRAAL:

- The telescope axis which can steered by an unwanted change in position of M3
- The Nasmyth adaptor rotation axis
- The GRAAL corotator axis

These 3 axes, not being co-aligned, a pupil run-out can be observed at the level of the 4 LGS WFS. To calibrate the pupil misregistrations, the following procedure is applied in commissioning:

- At each telescope elevation angle of interest
    - Stop telescope tracking which means that there is no motion of the Alt/Az axes
    - Acquire the 4 LGSs and close the jitter loop and then the HO loop
    - No NGS is required, which makes the process fairly quick
    - Scan the Nasmyth adaptor rotation angle range and compensate each angle with the corotator to keep the LSG WFSs coaligned with their LGS. The jitter and HO loop are opened and then reclosed right away when the angle is changed
- At each angle, the following telemetry is measured:
    - Closed loop slopes and DSM commands in order to retrieve a noisy IM
    - Closed loop WFS intensity vectors to calibrate a flux based method used for bootstrap
- A reference is also required to estimate the true misregistration at each position
    - The jitter loop is closed to keep the LGS spots centered
    - A full IM on sky is measured by fast push-pull of Hadamard modes [23]
    - A good SNR is reached in less than 1 mn

Figure 6 illustrates the situation at an elevation angle of 65°, when the reference measurement is considered. The pupil run out amplitude is larger than 1 subaperture size. The shape is a residual cardioid of different orientation and size for each LGS WFS. Changing the telescope elevation has an effect on the DSM flexures. Seen from the LGS WFS perspective, the result is a combination of shift and homothety of the cardioid, as can be seen on Figure 7 [left]. In summary, the witnessed misregistration, even though deterministic and reproducible, has a large amplitude and is not easy to model. Worst of all, the pupil motion is affected by M3 repositioning errors. At UT4's Nasmyth A, at the time of commissioning, M3 was not sufficiently reproducible. Thus, we have selected as a baseline strategy to track the misregistration online and regularly recompute and update the HO reconstructor. The misregistrations are estimated by means of a noisy IM retrieval from closed loop real time data without disturbance injection. To validate this strategy, the online IM is estimated with the previously acquired data at various elevation angle. The resulting estimated misregistrations are compared to the reference value provided by the IM on sky. Figure 7 [Right] shows a good agreement between the online estimate and the reference value with an accuracy of about +/- 20% of a subaperture, which is sufficiently accurate for the GLAO mode of GRAAL.

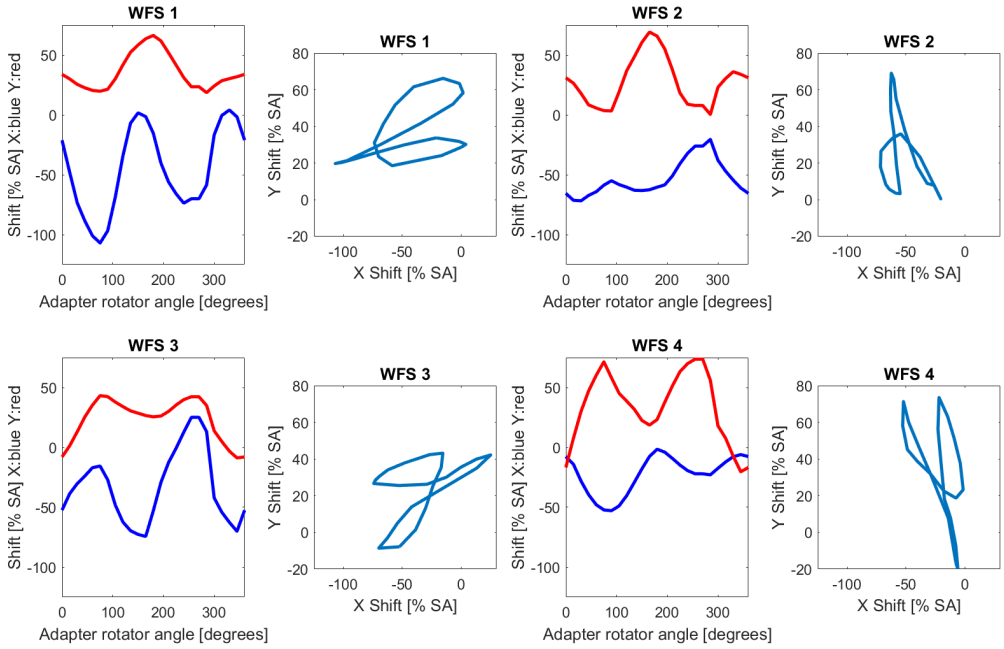

Figure 6: GRAAL - Elevation=65º - Reference misregistration measurement based on an on sky Hadamard IM

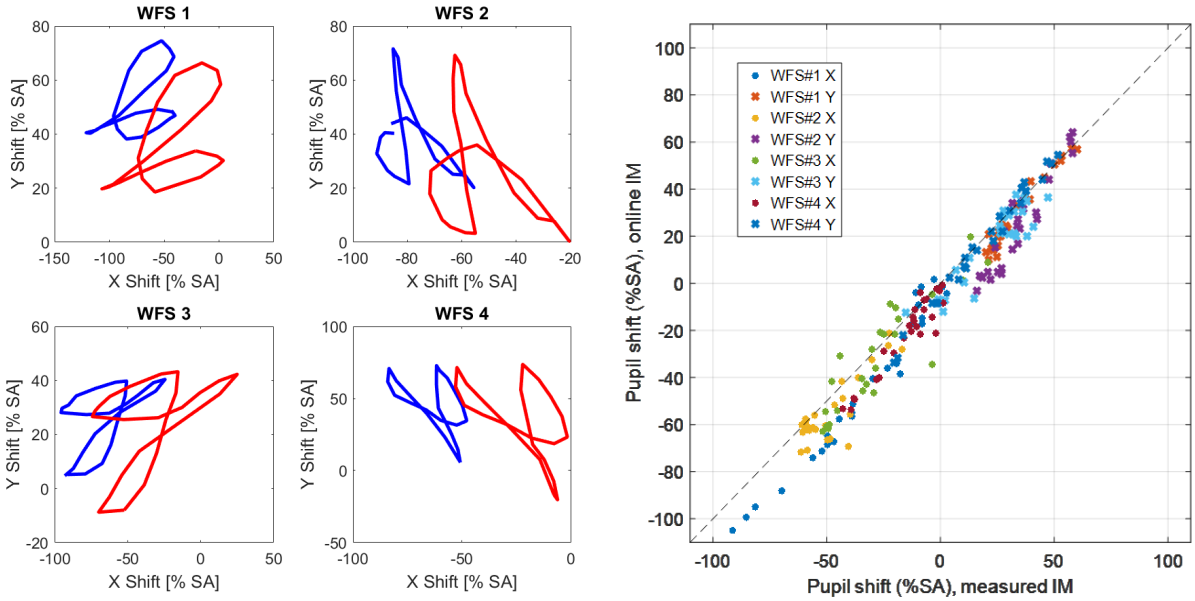

Figure 7: [Left] GRAAL - Reference misregistration at two elevation angles of 65 and 80º [Right] online pupil shift estimate based on the noisy IM retrieval against pupil shift estimated with high SNR on sky IM

The online IM approach has been validated and baselined for GRAAL. However, this method is quite slow because of data accumulation (~ 1 mn), data processing (~2 mn) and CM computation (~ 1 mn). It is not possible to close the loop with more than 1 subaperture unknown shift. Therefore, a fast bootstrap is required.
We chose a method based on the flux balance across the subapertures, which can provide a fast assessment of the pupil position. However, the pupil shifts are so large that we decided not to consider only few subapertures at the right, left,

top and bottom edges. Instead, we developed a method based on a Principal Component Analysis (PCA) and a statistical selection of the dataset. The method consists in the following steps for a dataset of 60 measurements acquired at 3 different telescope elevations and various rotator angles:

- First, the selection algorithm of Kennard-Stone is used to determine a calibration dataset that spans uniformly the 8 dimensional space of Shift in X and Y for the 4 WFSs. This way, an optimal calibration set of 40 samples is determined. These samples will be used to build a misregistration model. The 20 other samples are used for an independent validation of the model. This is the validation set (see Figure 8). The Kennard-Stone algorithm simply selects a subset of samples which provide uniform coverage over the dataset in terms of geometric distance. It necessarily includes samples on the boundary of the dataset.
- The 1s averaged intensity vectors (length: 1240) corresponding to the calibration dataset are mean subtracted, then normalized by their standard deviation and finally concatenated in a matrix.
- A PCA algorithm is run on the calibration samples. Assuming that the diversity in the dataset is generated by the effect of misregistrations, the first 4 eigenvectors are selected because they represent 95% of the variance in the dataset.
- The 60 intensity vectors are then projected on these 4 eigenvectors by means of a scalar product.
- A multilinear regressive model is fitted on the 40 samples of the calibration set. The model quality is then verified on the validation dataset.

The misregistration estimations provided by this PCA based flux method are then compared to the reference misregistration value obtained from the high SNR on sky IM. The results are shown on Figure 9.
The validation residuals are never worse than 15 % of a subaperture, most of the time smaller than 5 %. If one considers all measurements (Calib+Valid, X and Y, 4 WFSs), there are 480 estimation to evaluate statistically the quality of the model. The result is summarized in the histogram shown in Figure 10 with a standard deviation of 3.7 % and an average bias of $-4e^{-3}$ %.
This bootstrap method is very fast (1s), non-invasive (no disturbance required) and accurate. Nevertheless, recently the prediction of one of the 8 axes drifted and became unreliable. The exact cause of this drift has not been investigated yet. It may be related to a bias inherent to any method based on flux as a change in the illumination pattern biases the measurement. We are now working on an alternative bootstrap scheme based on the measurement of a micro interaction matrix by actuating a few modes, those which are most sensitive to misregistration, essentially high spatial frequencies. This method will also be fast enough for a bootstrap and probably less biased than the flux method as it measures directly the signal of interest, that is to say the registration of the DSM actuator pattern with the lenslet array geometry.

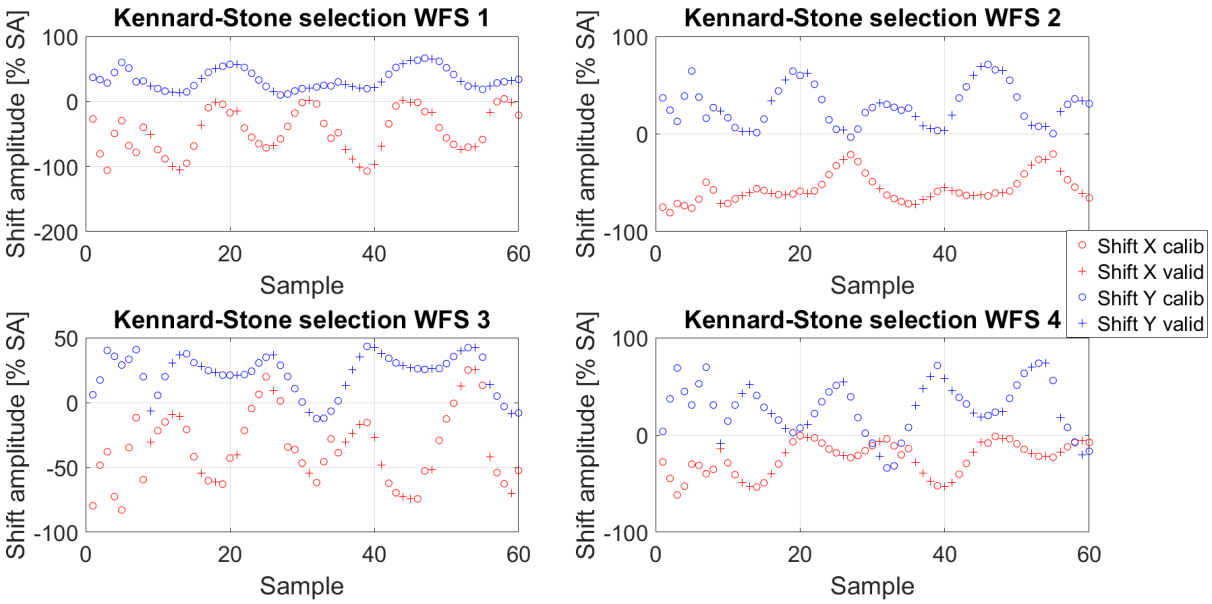

Figure 8: Kennard and Stone algorithm selecting 40 samples well distributed (in terms of geometric distance between the points) across the 8 dimensional parameter space of Shift in X and Y as seen by the 4 LGS WFS – [Circles] Calibration set [Crosses] Validation set

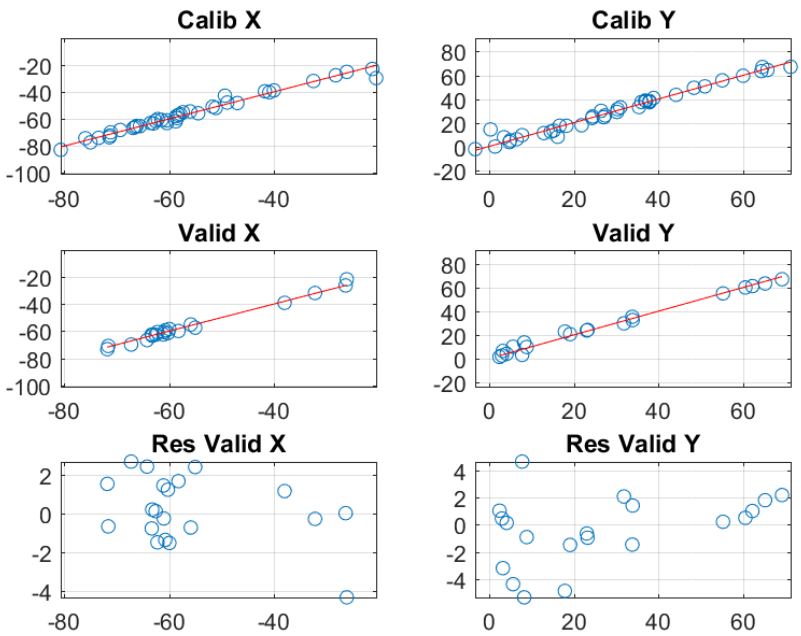

Figure 9: Misregistration estimation by PCA based flux method – LGS WFS4 – Estimated pupil shift against reference pupil shift

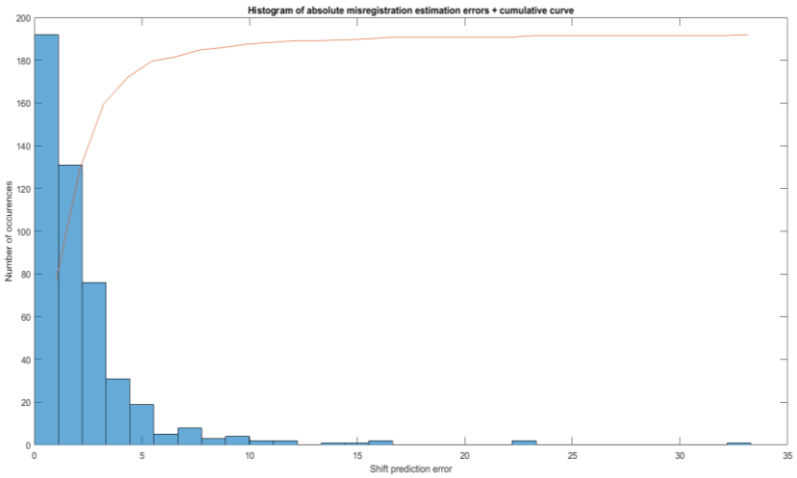

Figure 10: Histogram of pupil shift prediction error from the PCA based flux method

With GALACSI at Nasmyth B, the situation is different as shown on Figure 11. The amplitudes are smaller and there is a simple and reproducible law with respect to the elevation angle, for both WFM and NFM. For this reason, the baseline strategy for GALACSI is to use a Look-Up table of precomputed control matrices to be loaded depending on the telescope elevation angle.

The misregistrations showed to be very stable until September 2017 when a pure offset of 10 to 30% of a subaperture occurred. This was likely due to the fact that M1 and M2 were dismounted for recoating and maintenance. The misregistration law shall thus be recalibrated when such event occurs. The good news is that we do not need to use night time to recalibrate the misregistrations. Indeed, Figure 12 shows that the misregistration estimated by the online IM during observations is good enough, after outlier filtering, and matches well the reference measurement from a high SNR IM on sky. Thus, the online misregistration estimation provides reliable results which are recorded during every OB. When the estimated misregistration differs significantly from the current model, a flag is triggered to initiate the recomputation of the control matrix look-up table.

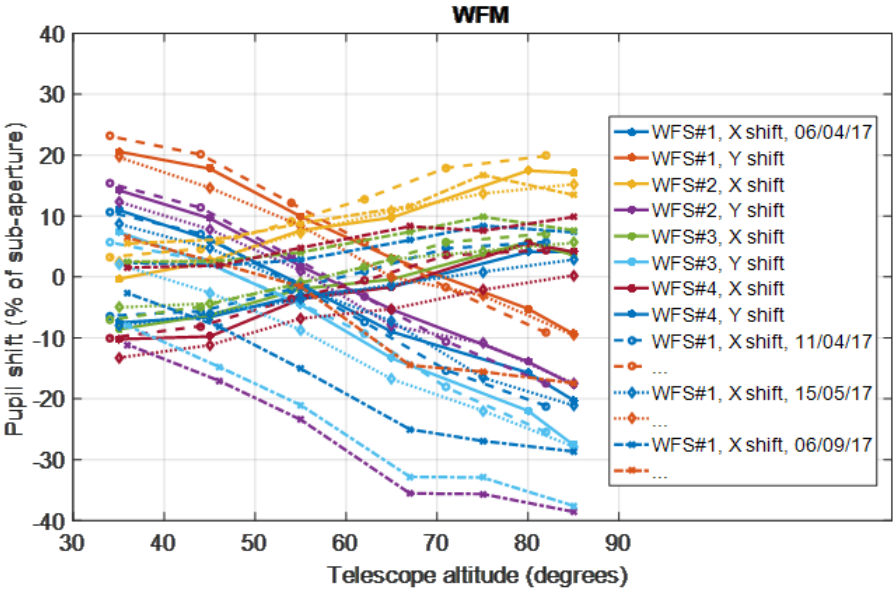

Figure 11: GALACSI WFM pupil shift measured for the 4 LGS WFS along X and Y

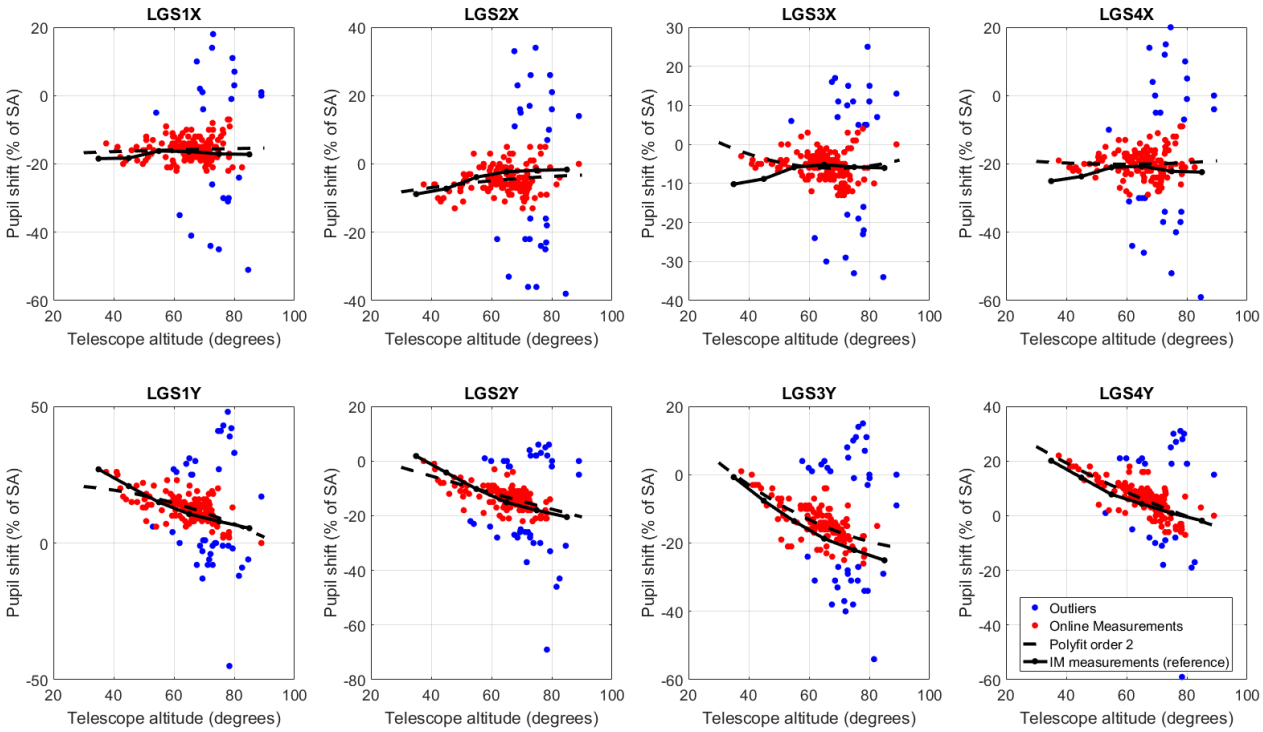

Figure 12: GALACSI NFM misregistration estimated with the online IM method (red) and the on sky IM measurement (black solid line) – [Top] X axis [Bottom] Y axis [Left to Right] LGS WFS 1,2,3 and 4

4.3 LTAO reconstructor model

The LTAO model is based on the pseudo-synthetic IM approach but goes beyond the interaction between the DSM and the 4 LGS WFSs. The method to build the GALACSI NFM's LTAO reconstructor has been described in detail in [27].

Using the schematic representation shown in **Figure 13**, let us recall the main computation steps:

- By applying KL modes in the ground layer and several altitude layers, a PSIM is computed between each layer and the 4 LGS WFSs, simulating the LGS beam cone at a given telescope elevation. The WFS model includes the misregistrations and accounts for the vector of valid subapertures. This step generates an "MCAO" *IM*.
- The ground layer IM can be inverted to generate the *GLAO CM* with typically 550 controlled modes.
- The inversion of the "MCAO" IM generates an *"MCAO" CM* that transforms the LGS WFS slopes into a phase estimation in each layer. The tomography reconstruction lies in the Minimum Mean Square Error (MMSE) inversion. Priors on turbulence covariance and measurement noise are used to regularize the inversion as described in [27]. However, the open loop priors being applied to closed loop residuals, unlike with the optimal Pseudo Open Loop Control (POLC) scheme [28], an hyper-parameter n_{phot} is used to tune the regularization. n_{phot} impacts the noise term. When n_{phot} is larger, the noise variance prior is lower which means that more confidence is given to the measurements, leading to a more aggressive tomography reconstruction with larger modal gains applied to the higher order modes, especially in the altitude layers. The tuning of this essential parameter will be discussed later.
- A virtual and perfect WFS is introduced on axis, where we want to optimize the correction. A synthetic IM *P* is computed between each layer and this on axis WFS, looking at an NGS with a cylindric beam geometry. *P* transforms the 3D turbulent phase into virtual WFS slopes on axis.
- A synthetic IM is computed between the DSM actuator geometry and this on axis WFS. It is inverted to generate the *"SCAO" CM* controlling a tunable number of DSM KL modes, typically 750 in LTAO.
- Multiplying *P* and *"SCAO" CM* generates a projector from the 3D turbulent phase onto the DSM commands.
- Finally, the multiplication of this projector with the *"MCAO" CM* provides the *"LTAO" CM* that transforms the LGS WFS slopes into DSM commands.

To get a reliable synthetic reconstructor, the geometry of the system has to be simulated properly. In other words, the relative positions of the LGS beam footprints in the altitude metapupils shall be simulated realistically. A signature of this geometry can be found in the LGS WFS slopes covariance matrix [29]. To enhance the patterns, let us consider on sky measurements acquired in WFM (2' diameter) in presence of a strong turbulence layer at 12km. This way, the overlap between the footprints being lower, the beam footprint signature appears more clearly in the covariance matrix. Then, a similar slopes covariance matrix is generated by a Monte Carlo simulation of several pseudo-synthetic models, corresponding to different geometries. The LGS beam footprint geometry is then fitted to the measured covariance matrix. Furthermore, since there is an ambiguity between the altitude of the meta-pupil and the LGS angle on sky, the LGS angle is identified by another method. The average LGS radius on sky is found to be 10.35" based on the analysis of LGS acquisition camera images, corrected from the parallax.

Finally, a large number of parameters are tuned based on simulations, experience on the laboratory test bench ASSIST and optimizations performed on sky:

- Number of controlled DSM KL modes=750
- Elevation angle: update of the reconstructor every 5º
- Reconstructed layers = 4
- Altitudes=[0 3 9 14] km with prior C_n^2 fraction =[0.75 0.1 0.05 0.1]. These are the equivalent layers corresponding to the median C_n^2profile at Paranal.
- Number of calibrated KL modes per layer=[1156 700 600 400]
- Prior r_0=0.1 m
- Noise variance prior tuned with hyperparameter n_{phot}

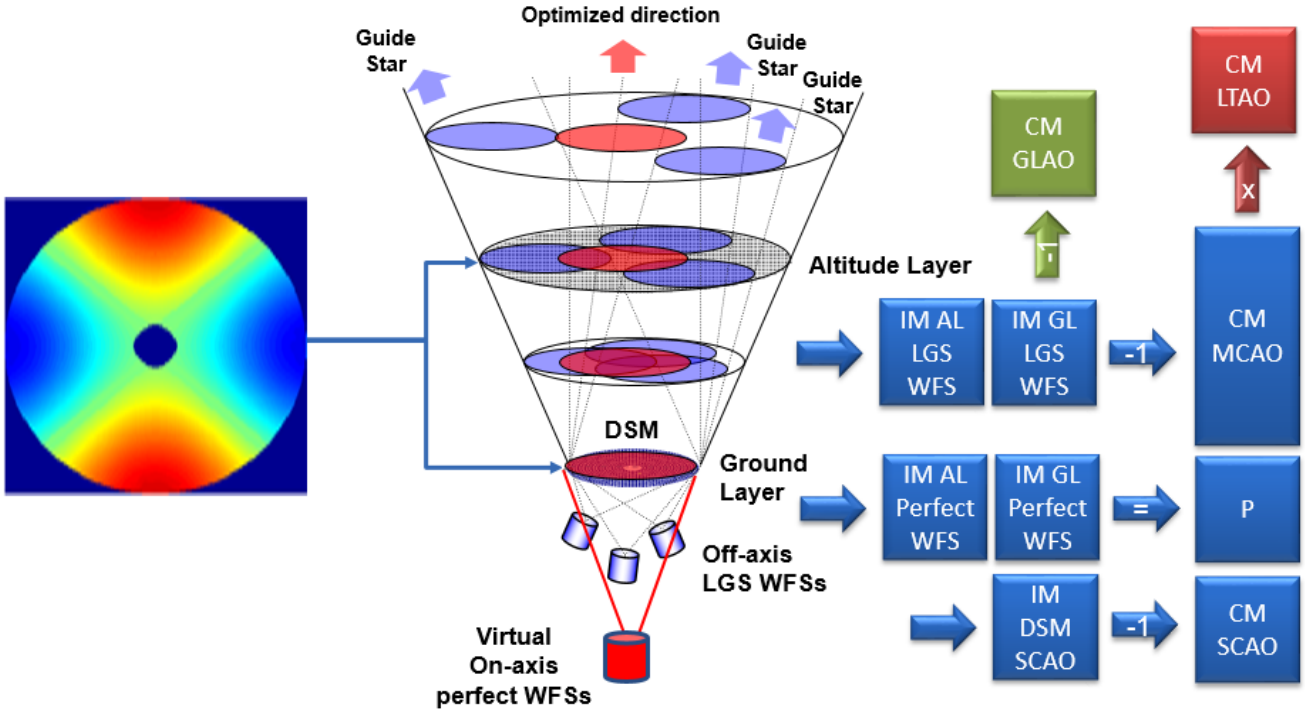

Figure 13: LTAO synthetic model – schematic representation

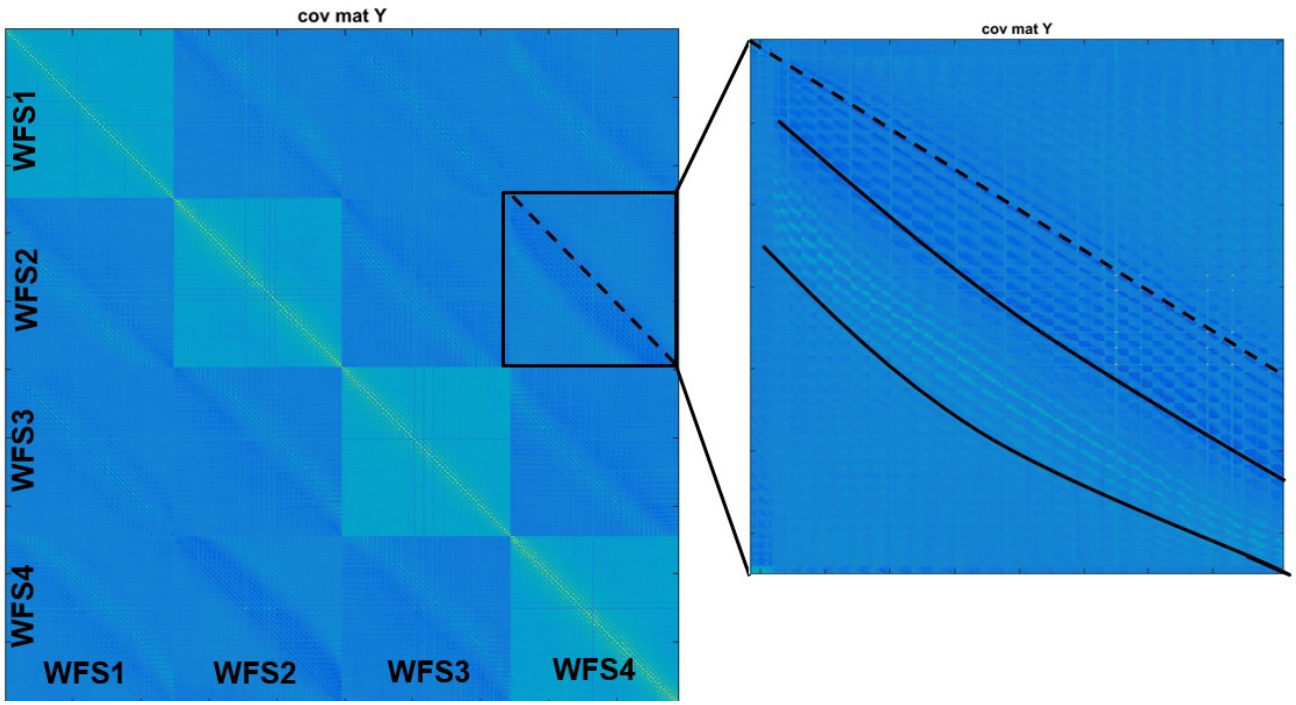

Figure 14: [Left] LGS WFS Y slopes covariance matrix extracted from a sequence of slopes measured on sky in WFM with a significant turbulence layer at 12km [Right] Zoom on the type of pattern to be fitted by the model

4.4 Tuning of regularization parameters

The regularization parameters have been verified on sky by scanning the turbulence covariance and the noise covariance priors as well as the integral gain. While the hyperparameter n_{phot} was expected to be around 1 based on laboratory tests experience, we consistently found that the MMSE had to be more strongly regularized. Figure 15 shows a typical result where n_{phot} is close to be optimum around a value of 0.5. The GLAO reconstructor performance is shown with a diamond symbol for n_{phot}=0, as a reference. This plot shows that the regularization tuning is sensitive and that it is hard to outperforms the GLAO reconstructor with a narrow LGS asterism.

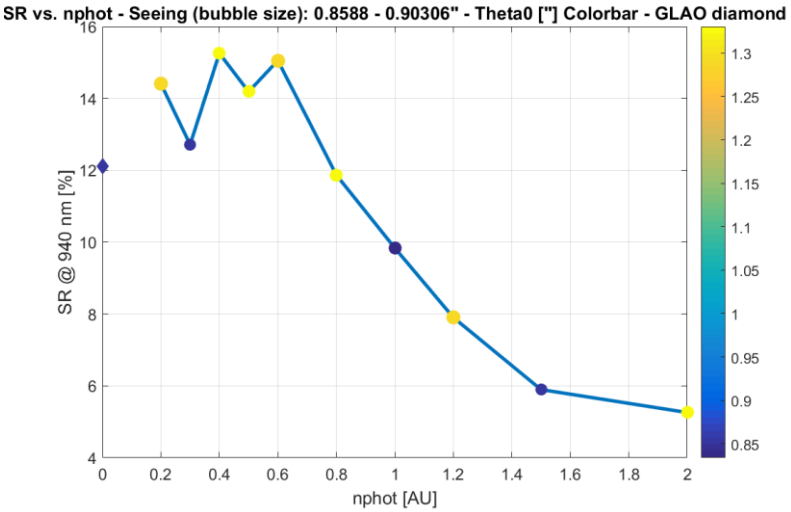

Figure 15: On axis Strehl ratio measured on the commissioning camera at 90 nm against the hyperparameter nphot - The seeing (bubble size) and the isoplanatic patch (colormap) are quite stable during the measurement. The GLAO reconstructor is shown for nphot=0 (diamond)

With n_{phot}=0.5, the regularization is so strong that the modal gains are dropping quickly with increasing spatial frequencies in each reconstructed layer as can be seen on Figure 16. The measured rejection transfer function shows that the modal gain for the KL mode number 100 is 0.16, which is significantly lower than the expected value of 0.33. The need for such strong regularization probably comes from an imperfect model of the system, especially in the metapupils where the tomography error occurs, which does not allow to reconstruct many modes in altitude. A better tuning of the model geometry will be carried out in the next months.
Since the regularization hyper-parameter acts on the noise term, it influences all reconstructed layers in the same way. Thus, the ground layer reconstruction quality is penalized in order to regularize properly the altitude layers. To improve the situation, the power law of the turbulence covariance in the ground layer is "fudged" (power law=1.5) in order to increase the prior variance of the higher order modes in the ground layer. The effect is a strong increase of the modal gains in the ground layer only. Finally, the rejection transfer function is restored to its expected behavior as shown on Figure 16.

5. PERFORMANCE AND ON SKY RESULTS

This section will report some first LTAO performance evaluation performed on sky during the first semester 2018. Illustrations of performance of the GLAO modes can be found in [30].

5.1 High-order loop performance

Once the LTAO reconstructor is tuned as described in the previous section, the LTAO reconstructor clearly outperforms the GLAO reconstructor provided there is sufficient turbulence energy in altitude as one can see on Figure 17. The low wind effect renders the commissioning data analysis difficult. Indeed, when looking at corrected PSF in the visible, even wind speed of about 6 m/s can generate sufficient differential piston around the telescope spiders to trigger PSF core explosions. To counter-act this effect during commissioning, targets were selected so that the telescope points towards the wind. In addition, for performance optimization, several PSFs were acquired by alternating several times between

different system tunings in order to account for the statistical impact of varying environmental conditions. For science operation, the low wind effect will be reduced to a low level of occurrence by an adhesive foil applied to the telescope spiders to reduce their emissivity. The installation of this foil is currently in progress at UT4.

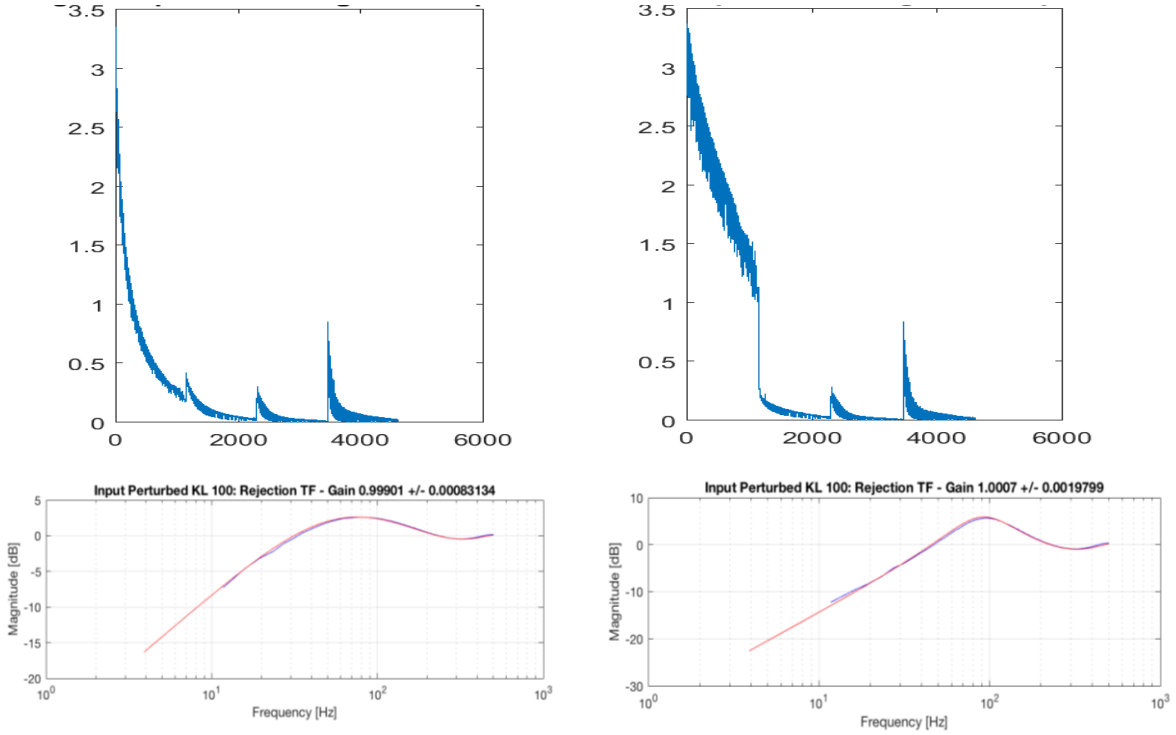

Figure 16: [Top] Modal gain as a function of mode number reconstructed by the MCAO CM. The 4 reconstructed layers appear [Bottom] Rejection transfer function measured on sky for the KL mode number 100 [Left] nominal turbulence covariance priors. The equivalent integral gain for the KL mode 100 is estimated to 0.16 [Right] Boosted prior covariance in the ground layer. The equivalent integral gain for the KL mode 100 is estimated to 0.33.

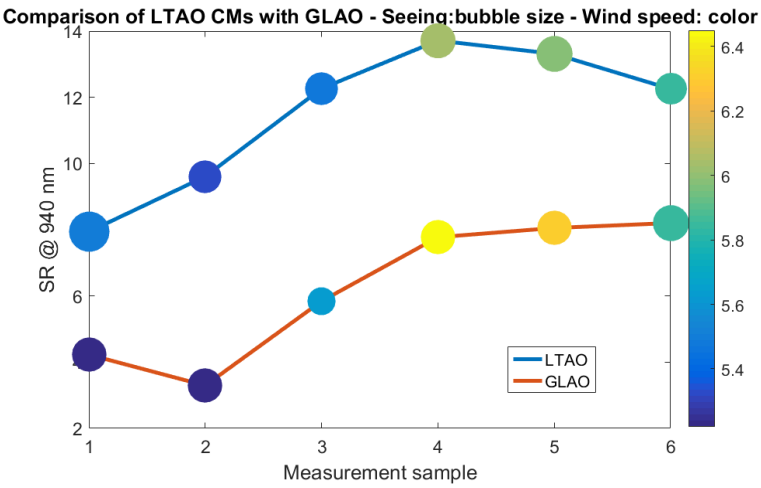

Figure 17: Strehl ratio measured with the commissioning camera @ 940 nm - 6 consecutive measurements of 30 s integration alternating between GLAO (red solid line) and LTAO (blue solid line) - During the measurement, the seeing (~ 0.55") and isolanatic patch (~1.3") are stable – Low wind effect becomes visible for wind speed < 6 m/s

Superb image quality could be obtained with MUSE in NFM. The resolution improvement is particularly striking when observing dense globular clusters or Galactic nuclei with patterned structures. MUSE was one of the most demanded

instrument of the VLT with a spatial resolution of 0.4" in the best conditions (no-AO). The GLAO mode now allows to increase the fraction of the time during which such resolution is available and even provides fwhm of 0.3" when the ground layer is strong. The LTAO mode opens the door to a new world in terms of spatial resolution. On MUSE data cubes, fwhm as low as 50 mas have been measured across the full spectral range from 500 to 930 nm. The LTAO mode of AOF basically provides a spatial resolution similar of better than the Hubble Space Telescope in the optical wavelength domain. Combining this resolution to the 3D spectral capability of MUSE enables unprecedented science. MUSE is now able to disentangle more than 10000 different objects in a field of 7.5 " square, measuring a spectrum with a resolution of ~ 3000 (depending on the wavelength slice) for each of these objects.

Unfortunately, the MUSE images cannot be shown in this paper as a press release is in preparation. So, we will now focus on images obtained with our visible commissioning camera. The advantage of this simple imager is that it does not suffer from the artefacts related to the reconstruction of an IFU image, consisting in stitching many different slices. Furthermore, the commissioning camera pixel scale is 5.6 mas while the MUSE spaxel is 25 mas. On the commissioning camera, with bright NGS, strehl ratios larger than 30% could be measured @ 940 nm and up to 20% @ 650 nm, while the fwhm ranges between 25 and 80 mas depending on the atmospheric conditions and NGS brightness

5.2 Examples of commissioning camera corrected images

Let us show a few examples of LTAO corrected image obtained during the first commissioning run in January 2018:

- On Figure 18, one can see the result of the first loop closure with GALACSI NFM. The seeing was about 0.5". The images were measured at 650 nm. The fwhm is improved from 340 to 34 mas when closing the loop.
- On Figure 19 is shown the correction obtained on a binary star separated by 2.6".
- On Figure 20, the correction radius is highlighted by looking at the PSF radial profile. In a case where the turbulence is mostly located at the ground, it is possible to regularize less, hence to push the modal gains of the higher order modes. In this case, the correction radius of about 300 mas is consistent with the correction of 750 KL modes. We have been able to control up to 1100 DSM modes out of 1150 degrees of freedom but this is not an optimal tuning with varying atmospheric conditions.

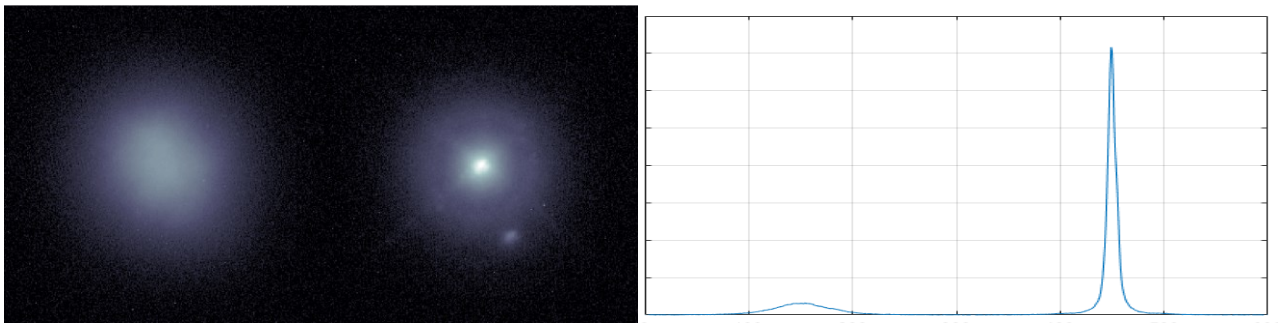

Figure 18:First GALACSI NFM correction obtained on the first commissioning night [Left] 650 nm PSF with AO loop opened (but telescope field stabilization on) and AO loop closed [Right] PSF profiles

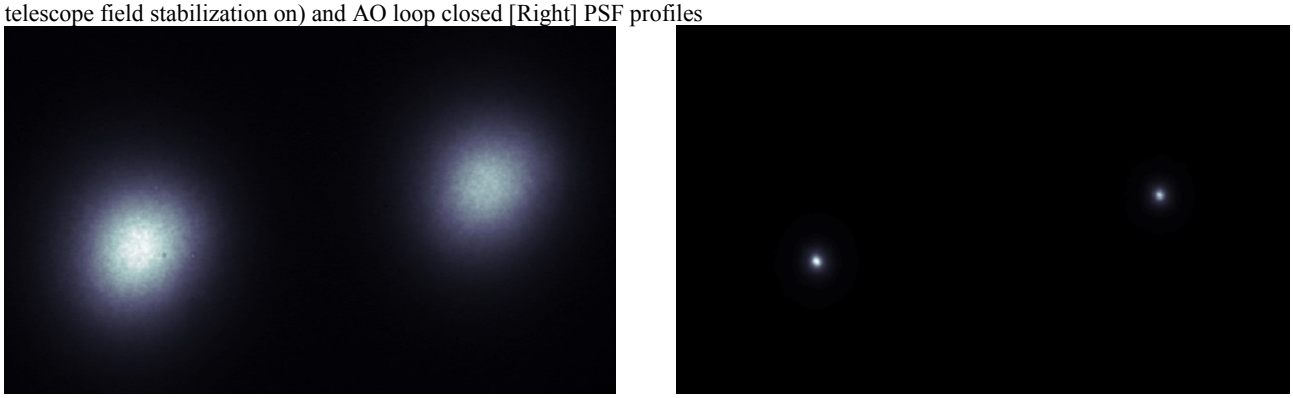

Figure 19: GALACSI NFM image at 650 nm of Hip 5508 (2.6" separation) [Left] seeing limited [Right] LTAO loop closed

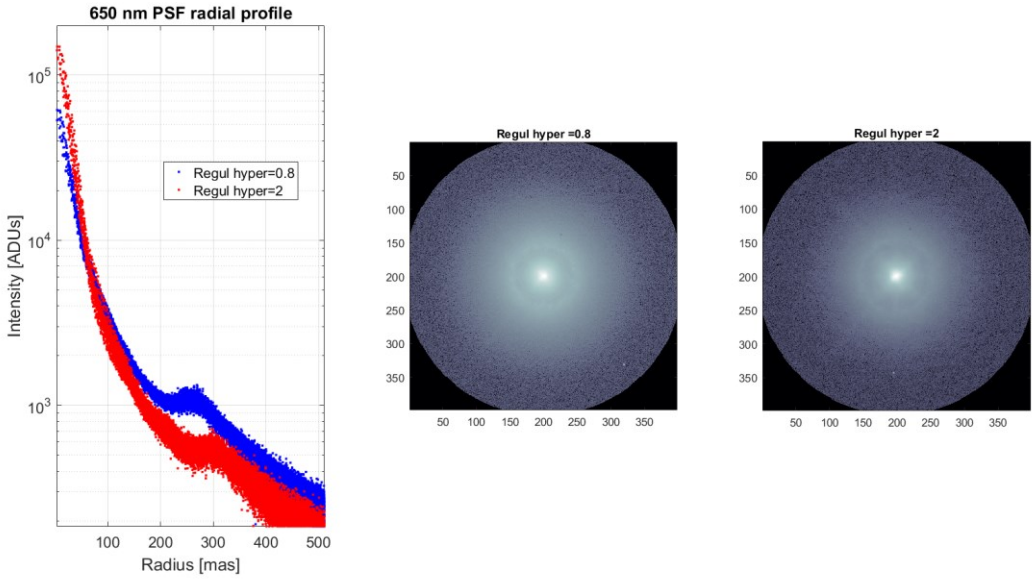

Figure 20: Impact of the regularization on the effective number of corrected modes, hence on the correction radius [Right] PSF obtained with an a low regularization [Middle] PSF obtained with a high regularization [Left] Logarithmic radial profile showing a clear improvement of the strehl ratio and an increase of the correction radius when regularizing less

It is important to note that the non-common path aberrations of the commissioning camera and MUSE have not been calibrated out. This is the case for all the images shown here. Furthermore, the presented strehl ratios are absolute and computed on long exposures, by counting photons across the full available field of view.

5.3 Faint NGS regime

The remaining outstanding issue with GALACSI NFM is the performance around the faint NGS regime. On Figure 21, the left plot shows the strehl ratio measured at 650 nm on the commissioning camera images (squares) and in the corresponding slice of the MUSE cube (circles) as a function of seeing along the line of sight. These datasets acquired during two distincts commissioning run show a good agreement between the strehl ratio computed with the well sampled commissioning camera and the undersampled MUSE reconstructed image. The strong impact of seeing on the performance in the visible is expected. The black solid line corresponds to an end-to end simulation of the system performance at the expected limiting magnitude of 15 in H band, with error budget. It is interesting to see that the data samples corresponding to NGS fainter than magnitude 13 (yellowish points) exhibit a performance drop which is too fast against seeing, while most blue dots corresponding to bright NGS cases are less sensitive to seeing and remain on the right side of the black curve reaching a good strehl ratio even for not so good seeing cases. The right plot confirms this sudden performance drop at an H magnitude of about 14, the current limiting magnitude being around 14.5 in H.

6. NEXT STEPS

Several sources of misalignment of the NGS WFS have been identified meanwhile. A pupil shift of about 10% of the diameter is combined to a pupil run-out of about 3% of the diameter. Furthermore, there is a significant defocus of the detector with respect to the lenslet array that yields a spot size enlargement which significantly reduces the measurement SNR. A realignment mission is planned for the beginning of 2019. Analytical simulations suggest a potential gain of 0.5 to 1 magnitude.

Furthermore, a detector upgrade is currently under evaluation at ESO, to replace the Hawaii1/ 11 e- RON detector by a aAPDarray SAPHIRA [31] sub-electron RON detector. Analytical and end-to-end simulations agree on an anticipated gain of another 2 to 2.5 magnitudes depending on the thermal and sky background noise. Pushing the limiting magnitude of GALACSI NFM to 17 in H band would offer to the scientific community interested in extra galactic science many

more observable targets. If one considers the particular case of quasars, almost none of them is brighter than magnitude 14 while several thousands have been identified as brighter than H magnitude 17. To be continued …

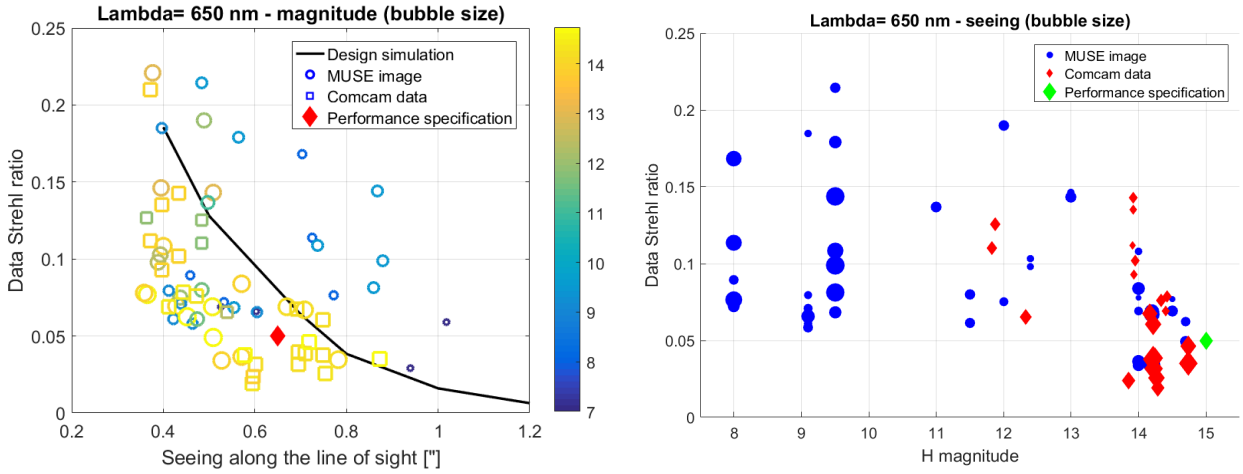

Figure 21: [Left] Strehl ratio measured at 650 nm with the commissioning camera (squares) and directly on the MUSE images (circles) against seeing along the line of sight. The colormap and the bubble size encodes the NGS H magnitude [Right] Strehl ratio measured at 650 nm with the commissioning camera (red diamonds) and directly on the MUSE images (blue circles) against H magnitude. The bubble size encodes the seeing along the line of sight

REFERENCES

[1] Arsenault R., et al., "Progress on the VLT Adaptive Optics Facility", ESO Messenger No.142, p.12 (2010)

[2] Arsenault R., et al., "Adaptive Optics Facility Status Report: When First Light Is Produced Rather Than Captured", ESO Messenger No. 164, p. 2 (2016)

[3] Arsenault R., et al., "The Adaptive Optics Facility: Commissioning Progress and Results", ESO Messenger No. 168, p.8 (2017)

[4] ESO Announcement, "First Light for Largest Adaptive Optics System - VLT Unit Telescope 4 takes a key step towards being fully adaptive", ann16078 (October 28th, 2016)

[5] Hackenberg, W. K., Bonaccini Calia, D., Abbad, J. A., Alvarez, J. L., Beltran, J., Buzzoni, B., Comin, M., Del Valle, D., Duhoux, P. R., Dupuy, C., Fischer, G., Gago Rodriguez, F., Guzman, R., Haguenauer, P., Haimerl, P., Holzlöhner, R., Huber, S., Kern, L., van Kesteren, A., Kirchbauer, J. P., Kuntschner, H., Lewis, S., A., Lizon, J.-L., Madec, P.-Y., McLay, S., Munoz, I., Palacio, J. C., Pfrommer, T., Pirard, J.-F., Popovic, D., Quattri, M., Quentin, J., Ridings, R., Riquelme, M., "ESO 4LGSF: Integration in the VLT, Commissioning and on-sky results," Proc. SPIE 9909-27 (2016)

[6] Biasi, R., Andrighettoni, R., Angerer, G., Mair, C., Pescoller, D., Lazzarini, P., Anaclerio, E., Mantegazza, M., Gallieni, D., Vernet, E., Arsenault, R., Madec, P.-Y., Duhoux, P., Riccardi, A., Xompero, M., Briguglio, R., Manetti, M., Morandini, M., "VLT deformable secondary mirror: integration and electromechanical tests results," Proc. SPIE 8447, Adaptive Optics Systems III, 84472G (13 September 2012)

[7] Paufique, J., Madec, P.-Y., Kolb, J., Kuntschner, H., Argomedo, J., Kiekebusch, M. J., Donaldson, R. H., Arsenault, R., Siebenmorgen, R., Soenke, C., Tordo, S., Conzelmann, R. D., Jost, A., Reyes-Moreno, J., Downing, M. D., Valenzuela, J. J., Haguenauer, P., "GRAAL on the mountaintop," Proc. SPIE 9909-91 (2016)

[8] ESO Announcement, "Sharper Images for VLT Infrared Camera - Adaptive optics facility extended to HAWK-I instrument", ann18006 (January 30th, 2018)

[9] La Penna, P. Stroebele, S., Aller-Carpentier, E., Argomedo, J., Arsenault, R., Conzelmann, R. D., Donaldson, R. H., Gago Rodriguez, F., Gutierrez, P., Hubin, N., Jolley, P. D., Kiekebusch, M. J., Kirchbauer, J. P., Klein, B., Kolb, J., Kuntschner, H., Le Louarn, M., Lizon, J.-L., Madec, P.-Y., Mehrgan, L. H., Oberti, S., Quentin, J., Suárez Valles, M., Soenke, C., Tordo, S., Vernet, J. D. R., "AOF: standalone test results of GALACSI," Proc. SPIE 9909-114 (2016)

[10] ESO Press Release, “Cutting-edge Adaptive Optics Facility Sees First Light - Spectacular improvement in the sharpness of MUSE images”, eso1724 (August 2nd, 2017)
[11] Leibundgut B., et al., “MUSE WFM AO Science Verification”, ESO Messenger No. 170, p.20 (2017)
[12] Madec, P.-Y., Kolb, J., Oberti, S., Paufique, J., La Penna, P., Hackenberg, W. K., Kuntschner, H., Argomedo, J., Kiekebusch, M. J., Donaldson, R. H., Suárez Valles, M., Arsenault, R., “Adaptive Optics Facility: control strategy and first on-sky results of the acquisition sequence,” Proc SPIE 9909-37 (2016)
[13] Thomas, S. et al., Comparison of centroid computation algorithms in a Shack–Hartmann sensor, MNRAS (2006)
[14]]Kolb, J., Martinez, P., Girard, J. H. V., “What can be retrieved from adaptive optics real-time data?,”Proc. SPIE 8447-219 (2012)
[15] Neichel, B., Guesalaga, A., Gendron, E., Masciadri, E., Morris, T. J., Fusco, T., Vidal, F., Sivo, G., Osborn, J., Garrel, V., Rousset, G., Rigaut, F., Correia, C. M., Butterley, T., Oberti, S., Kolb, J., Madec, P.-Y., Lardière, O., Conan, J.-M., Robert, C., Ziad, A., Martin, O., Ono, Y. H., “Review on AO real-time turbulence estimation, “ Proc. SPIE 9909-16 (2016)
[16] Guesalaga, A. et al., “On-sky results of the AOF online profiler”, SPIE 10707-86 (2018)
[17] Pettazzi L., Fedrigo E., Muradore R., Haguenauer P. and Pallanca L., “Improving the Accuracy of Interferometric Measurements through Adaptive Vibration Cancellation”, IEEEMSC (2015)
[18] Deep, A., Arsenault, R., Boland, W., Delabre, B., Hubin, N., La Penna, P., Madec, P.-Y., Molster, F., Stuik, R., Tordo, S., Wiegers, E., “Alignment and integration of ASSIST: a test bench for VLT adaptive optics facility,” Proc. SPIE 7793, Optical System Alignment, Tolerancing, and Verification IV, 77930L (3 September 2010)
[19] Kolb, J., Madec, P.-Y., Arsenault, R., Oberti, S., Paufique, J., Stroebele, S., Donaldson, R, Soenke, Kiekebusch, M. J., Argomedo, J., Le Louarn, M., Vernet, J. D. R., Haguenauer, P.,Duhoux, P., Valenzuela, J. J., Guerra, J. C., “Laboratory results of the AOF System Testing,” Proc. SPIE 9909-105 (2016)
[20] Le Louarn, M., Madec, P.-Y., Kolb, J., Paufique, J., La Penna, P, Arsenault, R., Oberti, S., “Comparison between simulations and lab results on the ASSIST test-bench for the AOF,” Proc. SPIE 9909-277 (2016)
[21] Kolb, J., Madec, P.-Y., Le Louarn, M., Muller, N., Béchet, C., “Calibration strategy of the AOF”,Proc. SPIE 8447, 84472D (2012)
[22] Kolb, J., et al., “Review of AO calibration, or how to best educate your AO system”, Proc. SPIE 9909-20 (2016)
[23] Kasper, M., Fedrigo, E., Looze, D.P., Bonnet, H., Ivanescu, L., Oberti, S., “Fast calibration of high-order adaptive optics systems,” JOSAA, Opt Image Sci Vis., 21(6):1004-8 (June 2004)
[24] Oberti, S., Quirós-Pacheco, F., Esposito, S., Muradore, R., Arsenault, R., Fedrigo, E., Kasper, M., Kolb, J., Marchetti, E., Riccardi, A., Soenke, C., Stroebele, S., “Large DM AO systems: synthetic IM or calibration on sky?,” Proc. SPIE 6272, Advances in Adaptive Optics II, 627220 (28 June 2006)
[25] Esposito, S., Tubbs, R., Puglisi, A., Oberti, S., Tozzi, A., Xompero, M., Zanotti, D., "High SNR measurement of interaction matrix on-sky and in lab," Proc. SPIE 6272, Advances in Adaptive Optics II, 62721C (28 June 2006)
[26] Béchet, C., Tallon, M., Thiébaut, E. M., “Optimization of adaptive optics correction during observations: fast algorithms and system parameters identification in closed-loop,” Proc. SPIE 8447-84 (2012)
[27] Oberti, S., et al., “AOF laser tomography mode: reconstruction strategy and first test results”, Proc. SPIE 9909-68 (2016)
[28] Gilles, L., Ellerbroek, Brent L., “Split atmospheric tomography using laser and natural guide stars,” JOSAA, vol. 25, issue 10, p. 2427, September 2008
[29] Vidal, F. et al., “Tomography reconstruction using the Learn and Apply algorithm”, AO4ELT (2010)
[30] Madec, P.Y. et al, “Adaptive Optics Facility: From an amazing present to a brilliant future… “, SPIE 10703-03 (2018)
[31] Finger, G. et al., “Development of the near-infrared eAPDarray SAPHIRA achieving sub-electron read noise at millisecond full-frame readout,” Proc SPIE 9909-40 (2016)